Supplement of Atmos. Chem. Phys., 22, 9843–9857, 2022
https://doi.org/10.5194/acp-22-9843-2022-supplement

Supplement of

Functionality-based formation of secondary organic aerosol from *m*-xylene photooxidation

Yixin Li et al.

Correspondence to: Renyi Zhang (renyi-zhang@tamu.edu)

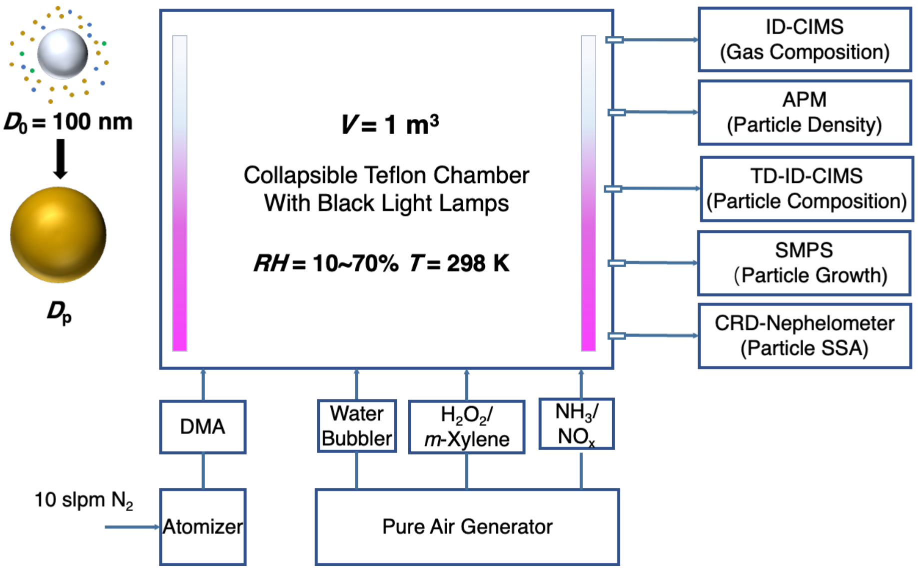

Figure S1. Schematic representation of the experimental setup. DMA for differential mobility analyzer; ID-CIMS for ion drift – chemical ionization mass spectrometry; APM for aerosol particle mass analyzer, TD-ID-CIMS for thermal desorption – ion drift – chemical ionization mass spectrometry; SMPS for scanning mobility particle sizer; and CRD for cavity ring-down spectroscopy. Monodispersed seed particles consisting of ammonium bisulfate, ammonium sulfate, and sodium chloride were exposed to oxidation products between m-xylene by OH and in the absence/presence of NH_3 vapors inside a 1 m^3 reaction chamber. RH was regulated between 10% and 70%, and T was maintained at 298 K. The gaseous concentrations of the oxidation products and particle properties, such as density, chemical composition, growth, and single scattering albedo, were simultaneously quantified by ID-CIMS, APM, TD-ID-CIMS, SMPS, and CRD-Nephelometer, respectively.

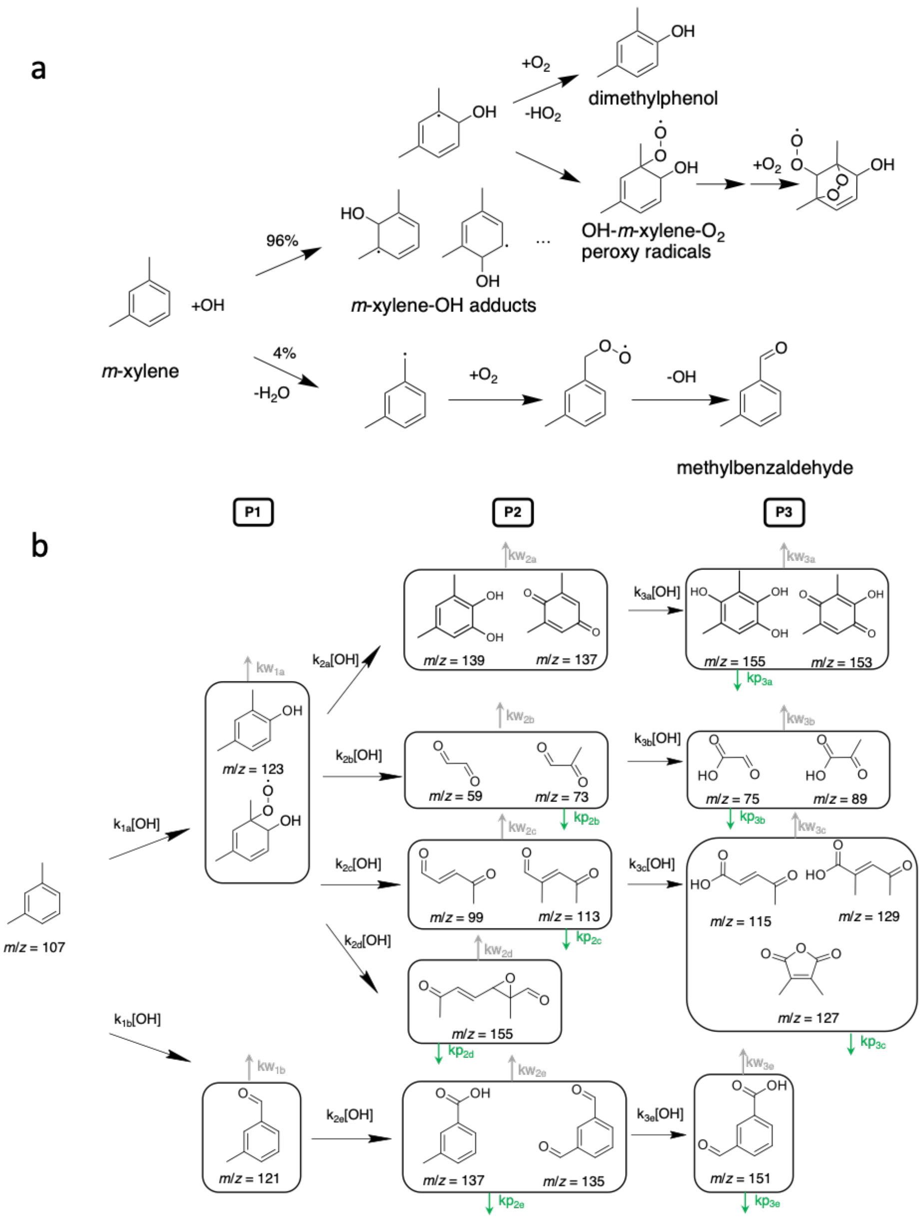

Figure S2. (a) The initial oxidation steps for OH oxidation of *m*-xylene leading to the formation of m-xylene-OH adducts, dimethylphenol, OH-m-xylene-O_2 peroxy radicals, and methylbenzaldehyde. (b) Multi-generation products from *m*-xylene-OH photooxidation. The letters of P1, P2, and P3 denote the products of first, second, and third generation of reactions with OH, respectively. The compounds in each box are lumped in kinetic simulation with the rate constant with OH (k_i), wall loss rate constant (kw_i), and uptake rate constant (kp_i) listed in Table S1. The numbers denote the mass to charge ratio (*m/z*).

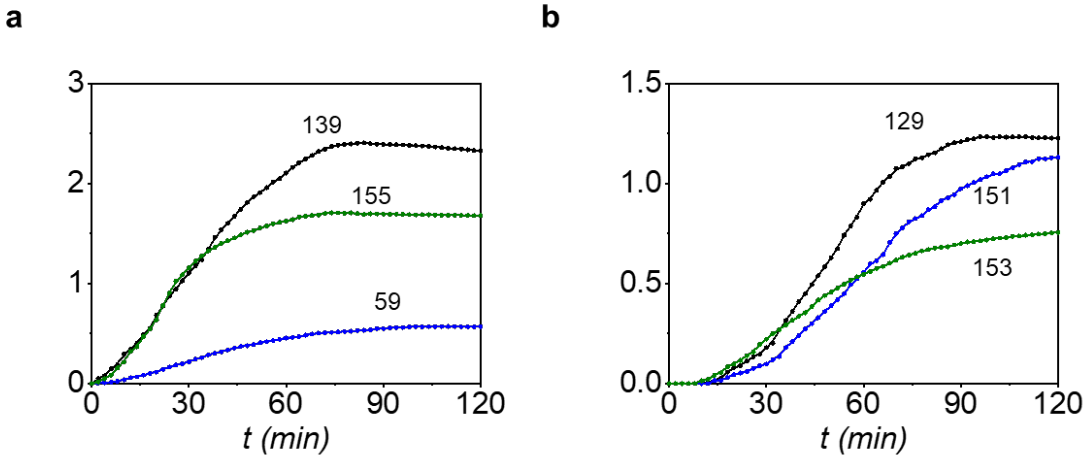

Figure S3. Temporal evolutions of additional P2 (a) and P3 (b) concentrations from *m*-xylene oxidation. The number denotes *m*/*z* value of the compound on ID-CIMS. The experiments were carried out on $(NH_4)_2SO_4$ seed particles with 19 ppb NH_3 and at 298 K and RH = 90%. Initiation of photooxidation by ultraviolet light occurred at *t* = 0.

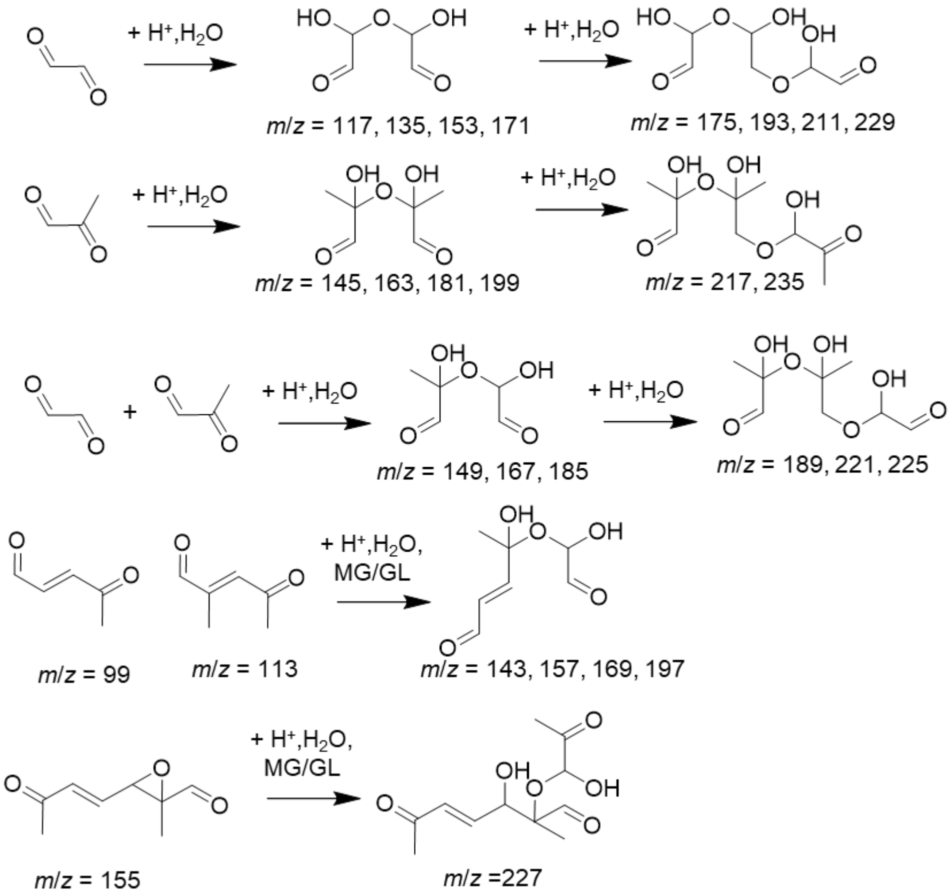

Figure S4. Pathways for oligomerization. The mechanisms leading to formation of particle-phase oligomers from α-dicarbonyls, γ-dicarbonyls, tricarbonyls, and epoxide detected by TD-ID-CIMS.

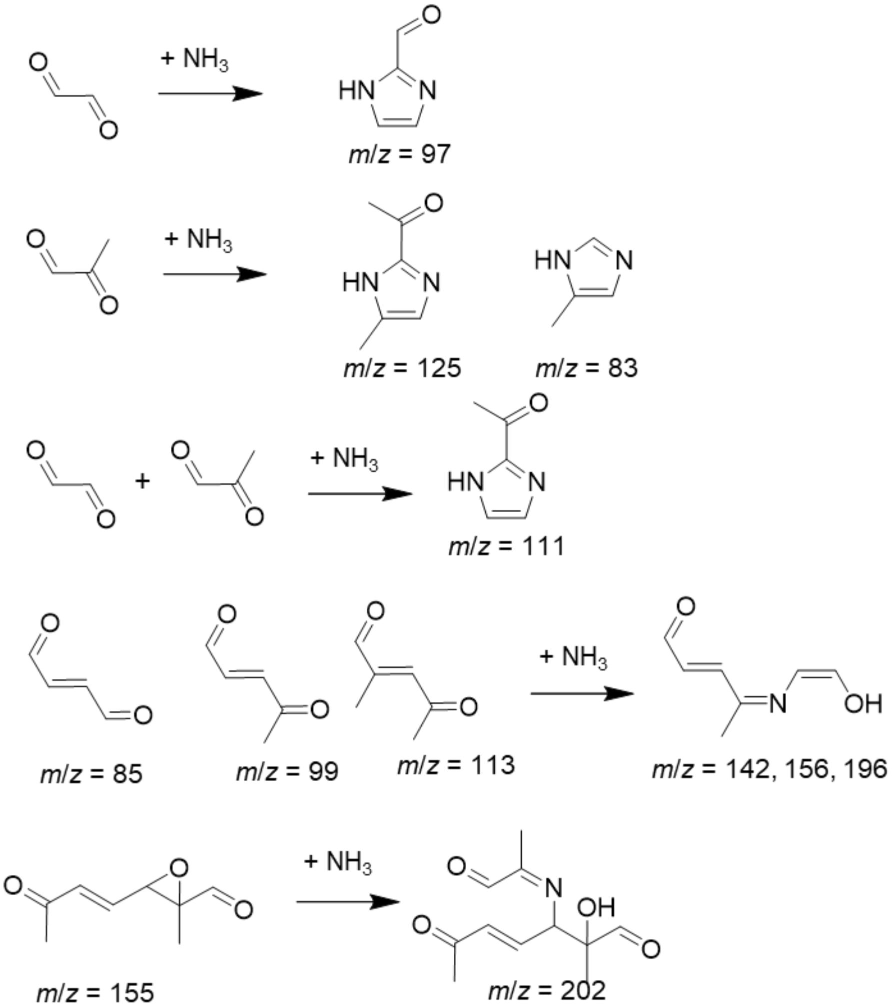

Figure S5. Pathway for BrC formation. The mechanisms leading to formation of particle-phase nitrogen-containing organics (NCO) from α-dicarbonyls, γ-dicarbonyls, tricarbonyls, and epoxide.

Table S1. Parameters for Kinetic model simulation of gas-phase concentrations. Reaction rate constants are taken from MCM V3.3.1 (Jenkin et al., 2003). The relations between products from each generation are provided in Figure S1b. $k'_n = k_n[OH]$ denotes the pseudo-first order rate constant of each oxidation step. $l_n = kw_n + kp_n$ is the overall loss rate of each species.

P1	**k_1 (×10^{-12} cm^3 molecule^{-1} s^{-1})**	**k_{w1} (×10^{-4} s^{-1})**	
1a	4.0	6.84	
1b	0.94	3.6	
P2	**k_2 (×10^{-12} cm^3 molecule^{-1} s^{-1})**	**k_{w2} (×10^{-4} s^{-1})**	**k_{p2} (×10^{-4} s^{-1})**
2a	38.2	1.8	
2b	25.5	13.1	16.3
2c	25.5	11.9	3.3
2d	6.7	12.9	3.5
2e	12.9	5.9	0.92
P3	**k_3 (×10^{-12} cm^3 molecule^{-1} s^{-1})**	**k_{w3} (×10^{-4} s^{-1})**	**k_{p3} (×10^{-4} s^{-1})**
3a	205	7.5	6.8
3b	360	5.0	3.3
3c	360	2.4	2.5
3e	12.9	6.3	0.92
C_1	$\frac{k'_1 k'_2 [A]_0}{(k'_3 + l_2 - k'_1)(k'_3 + l_2 - k'_2 - l_1)}$		
C_2	$\frac{k'_1 k'_2 [A]_0}{(k'_2 + l_1 - k'_1)(k'_3 + l_2 - k'_1)}$		
C_3	$\frac{k'_1 k'_2 [A]_0}{(k'_2 + l_1 - k'_1)(k'_3 + l_2 - k'_2 - l_1)}$		
C_4	$\frac{k'_1 k'_2 k'_3 [A]_0}{(k'_2 + l_1 - k'_1)(k'_3 + l_2 - k'_1)(k'_3 + l_2 - k'_2 - l_1)}(\frac{k_3 + l_2 - k_1}{k'_4 + l_3 - k'_2 - l_1} - \frac{k'_2 + l_1 - k'_1}{k'_4 + l_3 - k'_3 - l_2} - \frac{k'_3 + l_2 - k'_2 - l_1}{k'_4 + l_3 - k'_1})$		
C_5	$\frac{k'_1 k'_2 k'_3 [A]_0}{(k'_3 + l_2 - k'_1)(k'_3 + l_2 - k'_2 - l_1)(k'_4 + l_3 - k'_3 - l_2)}$		
C_6	$\frac{k'_1 k'_2 k'_3 [A]_0}{(k'_2 + l_1 - k'_1)(k'_3 + l_2 - k'_1)(k'_4 + l_3 - k'_1)}$		
C_7	$\frac{k'_1 k'_2 k'_3 [A]_0}{(k'_2 + l_1 - k'_1)(k'_3 + l_2 - k'_2 - l_1)(k'_4 + l_3 - k'_2 - l_1)}$		

Table S2. Mass peak assignments for oligomeric products detected by TD-ID-CIMS.

	m/z	MW	Formula
Methylglyoxal			
Dimers	145	144	$C_6H_8O_4$
	163	162	$C_6H_{10}O_5$
	181	180	$C_6H_{12}O_6$
Trimers	217	216	$C_9H_{12}O_6$
	235	234	$C_9H_{14}O_7$
	253	252	$C_9H_{16}O_8$
Glyoxal			
Dimers	117	116	$C_4H_4O_4$
	135	162	$C_4H_6O_5$
	153	180	$C_4H_8O_6$
Trimers	175	174	$C_6H_6O_6$
	193	192	$C_6H_8O_7$
	211	210	$C_6H_{10}O_8$
γ-dicarbonyls			
Monomers	85	84	$C_4H_4O_2$
	99	98	$C_5H_6O_2$
Dimers	143	142	$C_6H_6O_4$
	157	156	$C_7H_8O_4$
	169	168	$C_8H_8O_4$
	197	196	$C_{10}H_{12}O_4$
Epoxide	141	140	$C_7H_8O_3$
	155	154	$C_8H_{10}O_3$

Table S3. Mass peak assignments for nitrogen-containing organics (NCO) from α-dicarbonyls n-heterocycles and γ-carbonyls n-chains detected by TD-ID-CIMS.

m/z	MW	Formula	Compound
Methylglyoxal n-heterocycles			
83	82	$C_4H_6N_2$	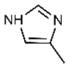
125	124	$C_6H_8ON_2$	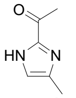
251	250	$C_6H_{10}O_5$	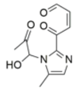
Glyoxal n-heterocycles			
69	68	$C_3H_4N_2$	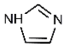
97	96	$C_4H_4ON_2$	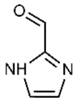
γ-carbonyls n-chains			
142	141	$C_6H_7O_2N$	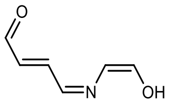
156	155	$C_7H_9O_2N$	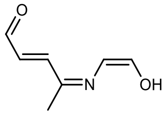
196	195	$C_4H_6O_2N_2$	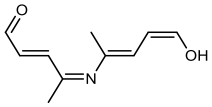

Table S4. Mass peak assignments for organic acids and PAQ detected by TD-ID-CIMS.

m/z	MW	Formula	Compound
89	88	$C_3H_4O_3$	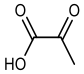
113	112	$C_5H_4O_3$	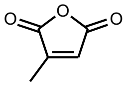
115	114	$C_5H_6O_3$	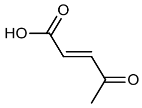
125	124	$C_7H_8O_2$	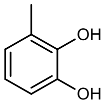
127	126	$C_6H_6O_3$	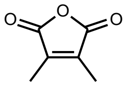 , 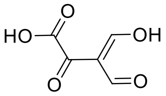
129	128	$C_6H_8O_3$	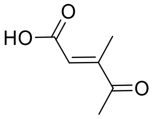
131	130	$C_5H_6O_4$	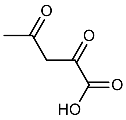
137	136	$C_8H_8O_2$	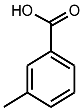
139	138	$C_8H_{10}O_2$	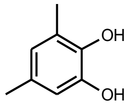
151	150	$C_8H_6O_3$	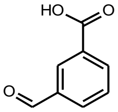
153	152	$C_8H_8O_3$	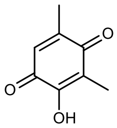
155	154	$C_8H_{10}O_3$	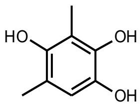
167	166	$C_8H_6O_4$	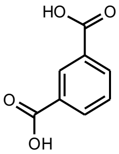
171	170	$C_8H_{10}O_4$	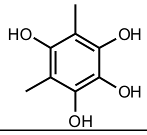

Table S5. The percent contributions of COOs from *m*-xylene-OH oxidation to the particle-phase mass intensity. GL: glyoxal, MG: methylglyoxal, GL+MG: cross-reaction of glyoxal and methylglyoxal. Note that the cross-reaction products of γ-carbonyls/tricarbonyls with α-dicarbonyls are summed into the contribution of γ-carbonyls/tricarbonyls. The experiments were carried on $(NH_4)_2SO_4$ seed particle with 19 ppb of NH_3.

Condensable oxidized organics	**Contribution**		
	Oligomerization	**NCO formation**	**Total**
GL	3%	3%	6%
MG	10%	12%	22%
γ-dicarbonyls	7%	8%	15%
epoxide	2%	0.3%	2%
Carboxylates			47%
PAQ			8%

Table S6. Saturation vapor pressures (P_s) of dicarbonyls, organic acids, and PAQ.

Compound	**p_s (atm, 298 K)**
Dicarbonyls	
Glyoxal	2.3×10^{-2}
Methylglyoxal	1.6×10^{-1}
Methylbutenedial	3.9×10^{-4}
Organic acids	
Toluic acid	1.1×10^{-5}
4-Oxo-2-pentenoic acid	6.6×10^{-6}
Acetylpyruvic acid	
Pyruvic acid	6.1×10^{-4}
Glyoxylic acid	1.9×10^{-3}
PAQ	
Dihydroxy dimethyl benzene	1×10^{-7}
Trihydroxy dimethyl benzene	8×10^{-9}
Hydroxy dimethyl quinone	3×10^{-7}

Table S7. Measured gaseous concentrations of condensable oxidized organics from *m*-xylene-OH oxidation at 10% and 70% RH.

m/z	**Average Concentration (ppb)**		**Ratio (R_c)**
	10% RH	70% RH	
Dicarbonyls			
59	1.3	0.51	2.8 ± 0.5
73	3.4	1.0	
99	4.2	1.7	
Carboxylate acids			
89	2.1	0.69	3.2 ± 0.8
113	4.1	1.6	
115	3.7	1.4	
117	2.0	0.52	
119	1.1	0.31	
127	3.3	1.18	
129	1.3	0.36	
137	0.42	0.19	
139	2.5	1.11	
143	1.5	0.40	
151	2.7	0.59	
153	0.66	0.35	
159	1.3	0.36	
161	0.97	0.25	
199	3.3	0.90	
PAQ			
155	0.47	0.23	1.9 ± 0.1
171	0.39	0.21	
187	0.3	0.16	
Nitrophenols			
154	1.4	0.7	2.6 ± 0.7
168	1.0	0.4	
184	0.5	0.15	
***m*-Xylene**			
Initial	1936	1936	
Final	1330	1363	

Table S8. Density of identified major SOA components by TD-ID-CIMS.

Compounds	***m/z***	**Density (g cm^{-3})**
Methylimidazole	83	1.03
Methylglyoxal	73	1.05
butenedial	85	1.06
4-Oxo-2-pentenoic acid	115	1.2
Imidazole	69	1.23
Pyruvic acid	89	1.25
Benzoic acid	123	1.27
Glyoxal	59	1.27
Dihydroxy toluene	125	1.29
Acetylpyruvic acid	131	1.3
Glyoxylic acid	75	1.38
Trihydroxy toluene	141	1.4
Glyoxal oligomers	175	1.71
2-hydroxy-5-methylquinone	139	1.4
Oxalic acid	91	1.9
Methylglyoxal oligomers	127	1.9

Table S9. Measured uptake coefficient (γ) for COOs on ammonium sulfate seed particles in the presence of ammonia. D_o = initial diameter, D_p = final diameter after the exposure time of dt, N = the particle number concentration, S = average particle surface area, and [A] = average concentration of species A. FR = percent contributions to the particle-phase mass intensity (Table S5).

Species	D_o (nm)	D_p (nm)	S (10^{-5} cm^2 cm^{-3})	[A] (ppb)	FR	γ (10^{-3})
RH = 70%						
Glyoxal	100.0	240.8	1.72	0.51	5.7%	8.0 ± 2.2
Methylglyoxal	100.0	240.8	1.72	1.0	22%	13 ± 3
γ-Dicarbonyls	100.0	240.8	1.72	1.7	11%	3.0 ± 0.5
Toluic acid	100.0	240.8	1.72	0.19	0.5%	1.0 ± 0.2
Pyruvic acid	100.0	240.8	1.72	0.69	3.6%	2.9 ± 0.4
4-Oxo-2-pentenoic acid	100.0	240.8	1.72	1.4	7.7%	2.5 ± 0.4
3-Methyl-4-Oxo-2-pentenoic acid	100.0	240.8	1.72	0.40	1.8%	2.2 ± 0.5
PAQ	100.0	240.8	1.72	0.60	8.0%	5.3 ± 1.8
Nitrophenol*	100.0	229.0	1.57	1.3	5.6%	1.7 ± 0.3
RH = 10%						
Glyoxal	100.0	310.0	2.31	1.3	0.9%	0.74 ± 0.30
Methylglyoxal	100.0	310.0	2.31	3.4	3.9%	1.0 ± 0.5
γ-Dicarbonyls	100.0	310.0	2.31	4.2	2.1%	0.37 ± 0.12
Toluic acid	100.0	310.0	2.31	0.42	0.6%	0.99 ± 0.21
Pyruvic acid	100.0	310.0	2.31	2.1	7.5%	2.8 ± 0.6
4-Oxo-2-pentenoic acid	100.0	310.0	2.31	3.7	12.2%	2.3 ± 0.5
3-Methyl-4-Oxo-2-pentenoic acid	100.0	310.0	2.31	1.3	4.1%	2.0 ± 0.5
PAQ	100.0	310.0	2.31	1.2	8.4%	4.6 ± 1.5
Nitrophenol*	100.0	303.5	2.20	2.9	8.2%	1.7 ± 0.2

* Measured in the presence of 100 ppb NO_x

Table S10. Average uptake coefficients (γ) over all identified species of each type of condensable oxidized organics from *m*-xylene-OH oxidation at 10% and 70% RH.

COO type	$\gamma\,(10^{-3})$	
	10% RH	70% RH
m-Xylene		
Dicarbonyls	0.7 ± 0.3	8.0 ± 3.7
Carboxylic acids	2.0 ± 0.7	2.1 ± 0.8
PAQ	4.6 ± 1.5	5.3 ± 1.8
Nitrophenols	1.7 ± 0.2	1.7 ± 0.3
Toluene		
Dicarbonyls	0.7 ± 0.2	7.8 ± 1.9
Carboxylic acids	1.8 ± 0.3	2.0 ± 0.4
PAQ	4.2 ± 1.5	5.0 ± 1.5
Nitrophenols	1.6 ± 0.3	1.6 ± 0.3